Quaternary Science Reviews 211 (2019) 208–221

Contents lists available at ScienceDirect

Quaternary Science Reviews

journal homepage: www.elsevier.com/locate/quascirev

A 40,000-year record of aridity and dust activity at Lop Nur, Tarim Basin, northwestern China

Jian Liu [a, *], Rujian Wang [b, **], Yue Zhao [a], Yi Yang [a]

[a] Institute of Geomechanics, Chinese Academy of Geological Sciences, Key Laboratory of Paleomagnetism and Tectonic Reconstruction, Ministry of Natural Resources, Beijing, 100081, China
[b] State Key Laboratory of Marine Geology, Tongji University, Shanghai, 200092, China

ARTICLE INFO

Article history:
Received 22 December 2018
Received in revised form
1 March 2019
Accepted 16 March 2019
Available online 1 April 2019

Keywords:
Aridification
Dust activity
Northern hemisphere cold event
Past 40 kyr
Lop nur paleolake
Tarim basin
Northwestern China

ABSTRACT

The Taklamakan Desert is a major dust source area for northwestern China. The history of aridification and sandstorm activity of the desert is recorded in the lacustrine sediments of the Lop Nur paleolake, on the eastern margin of the desert. In this study, we used accelerator mass spectrometry ^{14}C dating, the ln (Al/Ca) ratio, and the grain size of the non-biogenic fraction of sediment core KY01 taken from the center of Lop Nur to produce a ~40 kyr record of local climate change. During mid–late Marine Isotope Stage (MIS) 3, increases in the ln (Al/Ca) ratio, alluvial mud content, and atmospheric dust content, and a decrease in the dust storm content indicate an overall wet climate. During MIS 2, marked decreases in the ln (Al/Ca) ratio and alluvial mud content, especially during the Last Glacial Maximum and Heinrich event 1 cold interval, indicate lowered atmospheric temperatures, as also recorded in Greenland ice cores. During MIS 2, fluvial input to the site was reduced and almost ceased, suggesting extreme aridity at Lop Nur, very strong low-altitude winds, and frequent dust storms. During early MIS 1, the contribution of dust storms to the lake sediments fell gradually and was then relatively constant, even during the Younger Dryas cold interval. This result might be ascribed to the increased supply of meltwater from snow and ice to Lop Nur, representing a response to the rise in atmospheric temperatures during the deglacial, accompanied by strong high-level winds. During 9–7 kyr BP there was an increase in the input of sediment from sandstorms, and hence an increase in low-level wind strength, possibly relating to the 8.2 kyr BP cold event. From 7.0 to ~1.5 kyr BP there was a decrease in sandstorm input and thus a gradual weakening of the strength of low-level winds. However, after ~1.5 kyr BP the sandstorm input increased. Overall, we conclude that dust storm activity in the region of Lop Nur since 40 kyr BP has been controlled mainly by Northern Hemisphere cold events, with atmospheric dust providing a background sedimentary component that was dominant during warm intervals. Our findings contribute to an improved understanding of the dynamics of dust transport and to the history of dust activity and the lacustrine sedimentary record in northwestern China.

© 2019 Elsevier Ltd. All rights reserved.

1. Introduction

The Tarim Basin is the largest inland basin in northwestern China, and the Taklamakan Desert, in the central Tarim Basin, is a key region for studying the environmental history of central Asia (Yang et al., 2006). The Tarim Basin experienced drastic environmental changes during the Pleistocene. During the early to middle Pleistocene, a large paleolake existed in the Tarim Basin (Jäkel and Grunert, 2003; Pan et al., 2008). However, this lake disappeared during the middle to late Pleistocene because of the uplift of the Tianshan Mountains and the Tibetan Plateau, which block regional atmospheric circulation and prevent moisture reaching the interior of the Tarim Basin (Xia et al., 2007). The modern Taklamakan region is extremely arid, and high wind speeds occur throughout most of the year. Hence, this region is one of the main dust sources in northwestern China and even in central Asia (Wang et al., 2003; Tao et al., 2009; Liu et al., 2014). However, the processes and mechanisms of, and the relationships among, the

* Corresponding author. No. 11 South Minzudaxue Road, Haidian District, Beijing, 100081, China.
** Corresponding author. 309 Ocean Building, 1239 Siping Road, Shanghai, 200092, China.
E-mail addresses: jianliu686@163.com (J. Liu), rjwang@tongji.edu.cn (R. Wang).

https://doi.org/10.1016/j.quascirev.2019.03.023
0277-3791/© 2019 Elsevier Ltd. All rights reserved.

various factors that control dust production, mobilization, and transportation in the region are unclear and remain debated (Liu et al., 1994; Ma et al., 2006; He et al., 2011; Teng et al., 2015).

Paleolake sediments have a wide spatial distribution and are temporally continuous. In addition, they have a high sedimentation rate and therefore high temporal resolution, which are attributes that make such sediments useful for paleoenvironmental reconstruction (Kelts and Ding, 1992; Chen et al., 2000). The Lop Nur paleolake, on the eastern margin of the Tarim Basin, is the lowest-lying area in the Tarim Basin, and its sedimentary deposits document its evolution from a large paleolake to an arid desert today. Lop Nur and its sediments are well suited to reconstructing the paleoclimate and environment of the Tarim Basin as well as the evolution of lakes in arid areas (Wang et al., 2000). Recent field studies of Lop Nur have revealed that during the late Quaternary the gradual aridification of the area was interrupted by several abrupt wet events (Luo et al., 2009; Jia et al., 2012) that can be precisely correlated with climatic oscillations recorded in the GISP2 Greenland ice core (Luo et al., 2008). In addition, the local climate alternated between cold–wet and warm–dry, and it exhibited distinctive regional patterns that differed from those of monsoon-dominated regions (Dong et al., 2012). Previous studies of Lop Nur have focused mainly on paleoclimatic reconstructions based on sedimentary records (Wang et al., 2000; Luo et al., 2008; Dong et al., 2012), with less attention paid to sediment provenance and its relationship to climate change.

The grain-size distribution (GSD) of terrigenous sediments preserves information on provenance, transport, and sedimentation processes (McCave et al., 2006; Jonkers et al., 2009). Techniques such as the End-Member Modeling Algorithm (EMMA) developed by Weltje (1997), which can efficiently extract information about a single provenance or transport agent from a bulk-grain-size dataset, are important for determining material sources and sedimentary processes. The method assumes that each transport agent or sediment provenance is characterized by a unique and consistent GSD, which makes it possible to obtain geologically meaningful end-members from the bulk-sediment grain-size dataset (Weltje, 1997). Various EMMAs have recently become available, including AnalySize (Paterson and Heslop, 2015), BEMMA (Yu et al., 2016), DRS-unmixer (Heslop et al., 2007), and EMMAgeo (Dietze et al., 2012). Hateren et al. (2017) compared different EMMAs and further confirmed that EMMA analysis is a powerful tool for unmixing GSDs.

In this study, accelerator mass spectrometry (AMS) ^{14}C dating, grain-size analysis, and measurement of the ln (Al/Ca) ratio were performed on sediments of core KY01 taken from the central part of Lop Nur (Fig. 1). The GSDs were used to determine variations in sediment provenance. The overall aim of the study was to reconstruct the process of aridification and the history of dust activity at Lop Nur since ~40 kyr BP.

2. Regional setting

Lop Nur is located at the eastern margin of the Tarim Basin (39.5–41°N, 88–94°E) and is the lowest-lying depression in the basin, with an altitude of only 780 m (Fig. 1); hence, it serves as a sink for fluvial inputs from the Tarim, Kongque, and Qiemo rivers. Lop Nur is surrounded by the Altun Mountains to the south, the Tianshan Mountains to the north, the Beishan hills to the east, and the Taklamakan Desert to the west (Ma et al., 2008). Lop Nur was once a huge NE–SW-oriented lake, measuring ~210 km long and ~130 km wide and having an area of ~27,000 km^2 (Yan et al., 1998; Ma et al., 2008). However, the overdevelopment of agriculture and animal husbandry in the upstream regions of the Tarim and Kongque rivers during the mid-twentieth century resulted in the accelerated aridification of the Lop Nur area (Luo et al., 2008), and Landsat satellite images reveal that the lake dried up completely during the 1970s (Xia et al., 2007).

3. Modern climate of the Lop Nur area

The modern climate of the Lop Nur area is continental arid, characterized by low precipitation (~28 mm/yr), high evaporation (~1200 mm/yr) (Zhang et al., 1992; Liu, 1996; Yang et al., 2011), a marked diurnal temperature range, and strong winds, with more than 25 strong-wind days annually. Meteorological data from Ruoqiang County (Fig. 1A) show that in recent decades the annual mean air temperature at Lop Nur has been 11.8 °C. Precipitation occurs mainly in summer is only ~11.5 mm (Fig. 2A). The multiyear mean wind speed is ~2.5 m/s, with the maximum in spring and minimum in winter (Fig. 2B). The winds in the region are extremely strong and can reach ~40 m/s. Extremely windy days occur mainly in spring and seldom in winter (Fig. 2C). The surface wind is mainly from the ENE and to a lesser degree from the WSW (Fig. 2D; http://www.data.cma.cn).

4. Materials and methods

4.1. Materials

Sediment core KY01, which was examined in this study, was obtained from the central region of Lop Nur (40°27′19.37″N, 90°20′24.51″E; altitude 780 m) (Fig. 1B) and has a total length of 42 m. Here, we focus on the upper 7.10 m of the core. Overall, the sediments of the studied interval consist of clayey silt and sandy silt, with occasional black stripes that are 0.2–0.5 cm thick. The lithological variations are summarized in Fig. 3.

4.2. Laboratory methods

4.2.1. AMS ^{14}C dating

AMS ^{14}C dating was performed on 19 bulk-sediment samples (mean TOC content of >0.6 wt %), a plant seed (from 42 cm depth in the core), and a single piece of charcoal debris (from 366 cm depth) at the Beta Analytic radiocarbon dating laboratory, Miami, Florida, USA (Table 1). The AMS ^{14}C ages were determined on humic acid leached from the samples. The radiocarbon ages of bulk lacustrine sediment samples are commonly older than the actual ages because of contamination by older carbon and the mixing of sediment by the activity of aquatic organisms; consequently, age data are typically corrected for the carbon reservoir effect (Aravena, 1992; Zhao et al., 2010; Hou et al., 2012), which is critical for proving reliable age control in the present study region (Fan et al., 2014).

The reservoir-calibrated charcoal ^{14}C age (14,540 ± 140 yr BP) is 180 yr younger than the calibrated ^{14}C age of humic acid (14,720 ± 60 yr BP) from the same sampling depth. The calibrated ^{14}C age of charcoal is usually regarded as the authentic depositional age of the sediment at the same depth (Chen et al., 2001; Fan et al., 2014). Based on this assumption, we further calibrated the reservoir-calibrated AMS ^{14}C ages of humic acid by subtracting 180 yr. In addition, all AMS ^{14}C ages were calibrated to calendar years (cal yr BP) using the CALIB 7.0.4 program with the INTCAL13 model (Stuiver et al., 2017). The AMS ^{14}C dating results are listed in Table 1.

4.2.2. Grain-size analysis

The samples used for grain-size analysis were obtained from core KY01 at an average interval of ~3.5 cm (n = 207). Microscope examination indicated that the samples are composed largely of

Fig. 1. (A) Location of Lop Nur (LN) within the Tarim Basin, northwestern China and (B) sampling location of core KY01 at LN. The information on core BST04H from Bosten Lake is from Chen et al. (2006). ◆: sampling region of 132 eolian sand samples in southwestern LN (Hua et al., 2009). ■: sampling location of optically stimulated luminescence (OSL) samples from the paleolake strata in the central Taklamakan Desert (Yang et al., 2006). ▲: sampling location of OSL samples from the top of the paleolake succession at the southern margin of the Taklamakan Desert (Yang et al., 2006). Light yellow regions mark the distribution of desert; blue and dashed lines denote rivers and runoff, respectively.

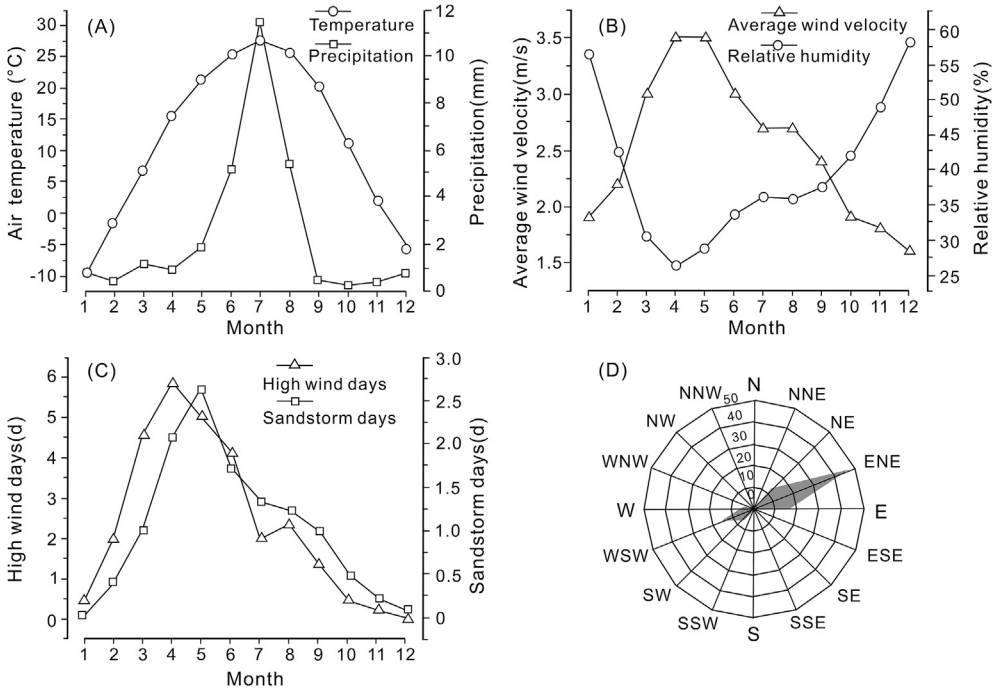

Fig. 2. Modern monthly mean meteorological data for Ruoqiang County. (A) Air temperature (°C) and precipitation (mm/month) for 1953–2012; (B) relative humidity (%) and wind speed (m/s) for 1953–2012; (C) high-wind days and sandstorm days (days) for 1971–2000; and (D) maximum wind speed and direction frequency diagram for 1980–2012. Data are from the National Meteorological Information Center of the United States (http://www.esrl.noaa.gov/psd/data).

quartz and feldspar (~95%), with minor chert, mica, rock fragments, and gypsum (<3 vol %). Prior to measurement, the samples were successively treated with 10 ml of H_2O_2 (10 wt %), 10 ml of HCl (1 moL/L), and 10 ml of NaOH (2 moL/L) to remove organic carbon, biogenic carbonate, and biogenic opal, respectively. The GSD of the non-biogenic components was then measured using a laser particle size analyzer (Beckman Coulter LS230) with a measurement range of 0.4–2000 μm at the State Key Laboratory of Marine Geology, Tongji University, Shanghai, China.

4.2.3. End-member modeling algorithm

EMMAs extract diagnostic data from GSDs, such as information

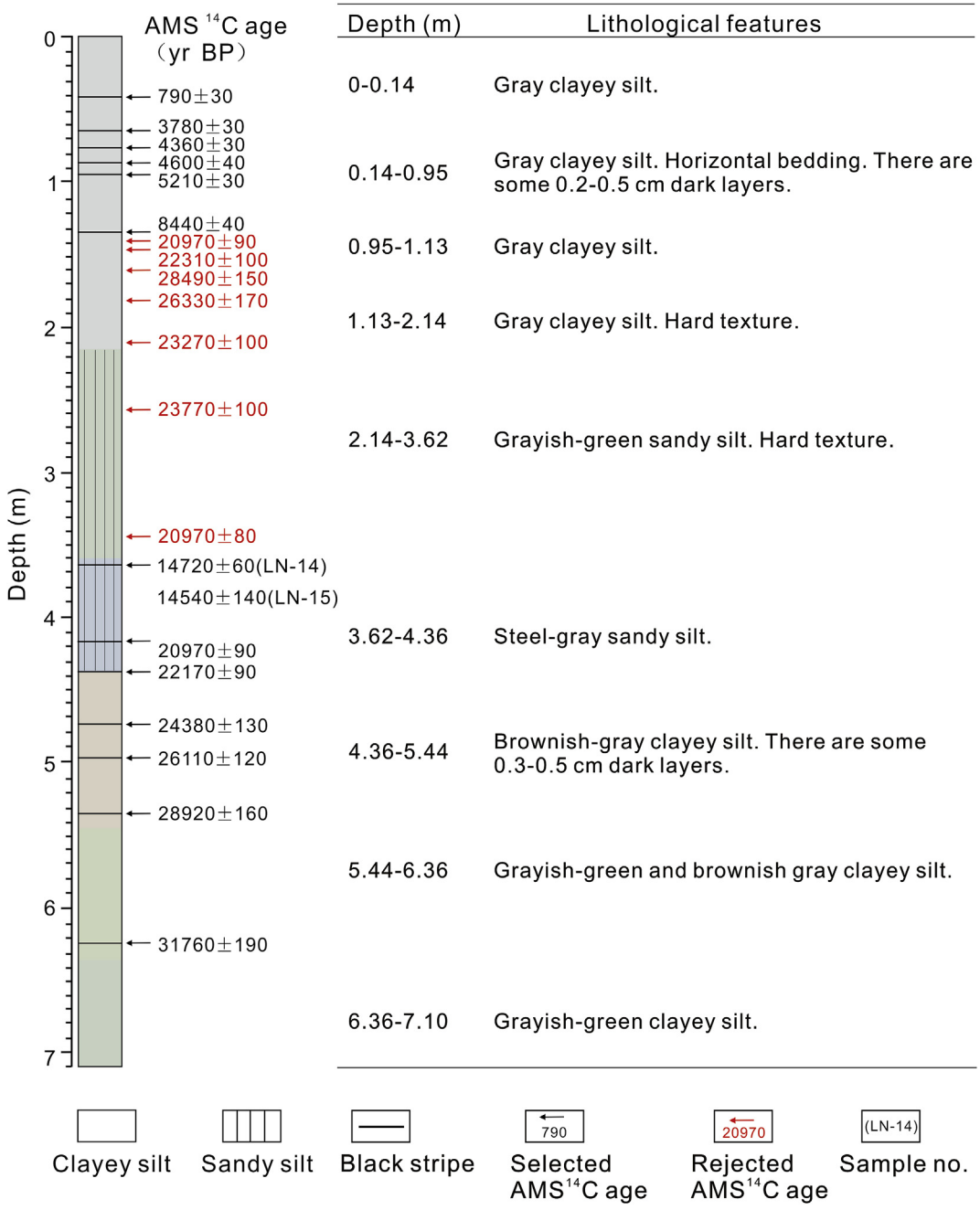

Fig. 3. Lithology and descriptions of sediments in core KY01 from LN, on the eastern margin of the Tarim Basin. Different colors in the columnar section indicate the sediment colors in the core. All calibrated ages (Table 1) are provided to the right of the lithological column. The legend is located at the bottom of the figure.

on provenance, transport, and sedimentation processes, which can subsequently be used to reconstruct past climatic variability. Hateren et al. (2017) conducted a comparative study of EMMAs and suggested that AnalySize (Paterson and Heslop, 2015) produced the best fit to grain-size frequency distributions. Therefore, we applied AnalySize software to our GSD data.

4.2.4. Al and Ca contents

Analyses of the sedimentary Al and Ca contents of core KY01 were performed on samples at an average interval of 7 cm (n = 100). Bulk-sediment samples were dried at 60 °C, finely ground, and heated at 600 °C for 2 h to decompose organic matter. The sediment samples, together with a series of Chinese and USGS rock and sediment standards, were then digested with a mixture of concentrated HF + HNO_3. The elements were measured by inductively coupled plasma–optical emission spectrometry (IRIS Advantage) at the State Key Laboratory of Marine Geology, Tongji University, Shanghai, China. Analytical precision and accuracy were monitored by replicate analyses of standards GSR-5, GSR-6, and GSD-9, yielding a relative standard deviation for the results of <1%.

5. Results

5.1. Age–depth model for core KY01

An age–depth model of the studied interval of core KY01 was

Table 1
Results of AMS^{14}C dating and age calibration of core KY01 from Lop Nur.

Sample no.	Lab I.D.	Depth (cm)	Dated material	AMS^{14}C age (yr BP)	^{14}C age corrected by 180 yr	Calendar age (yr BP)
LN-01	Beta 338841	42	Plant seed	790 ± 30		672–747
LN-02	Beta 316861	65	Humic acid	3780 ± 30	3600 ± 30	3838–3970
LN-03	Beta 315844	77	Humic acid	4360 ± 30	4180 ± 30	4614–4700
LN-04	Beta 313850	86	Humic acid	4600 ± 40	4420 ± 40	4867–5071
LN-05	Beta 313849	95	Humic acid	5210 ± 30	5030 ± 30	5709–5894
LN-06	Beta 316852	133	Humic acid	8440 ± 40	8260 ± 40	9119–9409
LN-07	Beta 316853	140	Humic acid	20,970 ± 90	20,790 ± 90	24,649–25379
LN-08	Beta 316854	147	Humic acid	22,310 ± 100	22,130 ± 100	26,060–26636
LN-09	Beta 316855	161	Humic acid	28,490 ± 150	28,310 ± 150	31,624–32759
LN-10	Beta 316856	182	Humic acid	26,330 ± 170	26,150 ± 170	29,886–30850
LN-11	Beta 316857	210	Humic acid	23,270 ± 100	23,270 ± 100	27,329–27713
LN-12	Beta 315846	259	Humic acid	23,770 ± 100	23,590 ± 100	27,526–27890
LN-13	Beta 315847	343	Humic acid	20,970 ± 80	20,790 ± 80	24,681–25370
LN-14	Beta 316858	366	Humic acid	14,720 ± 60	14,540 ± 60	17,530–17922
LN-15	Y-5	366	Charcoal debris	14,540 ± 140		17,530–17922
LN-16	Beta 316859	418	Humic acid	20,970 ± 90	20,790 ± 90	24,646–25379
LN-17	Beta 315849	438	Humic acid	22,170 ± 90	21,990 ± 90	25,790–26466
LN-18	Beta 313851	476	Humic acid	24,380 ± 130	24,200 ± 130	27,895–28581
LN-19	Beta 315845	499	Humic acid	26,110 ± 120	25,930 ± 120	29,721–30624
LN-20	Beta 316860	534	Humic acid	28,920 ± 160	28,740 ± 160	32,266–33444
LN-21	Beta 315848	622	Humic acid	31,760 ± 190	31,580 ± 190	34,987–35949

Note: reservoir calibration was conducted using CALIB7.0.4 (Stuiver et al., 2017).

constructed based on Bayesian methods (Blaauw et al., 2011; 2018) (Fig. 4). A comparison of AMS ^{14}C ages of the lake organic carbons in this core reveals that seven of the AMS ^{14}C ages of humic acid from depths of 140–343 cm (sample nos. LN-7 to LN-13, solid symbols in Fig. 4) appear anomalously old compared with the other ages, and they are relatively invariant with depth. Notably, the ^{14}C age (~25 kyr BP) at 343 cm depth (sample no. LN-13) overlaps with the ^{14}C age (~25 kyr BP) from 418 cm depth (sample no. LN-16) (Table 1). Thus, we conclude that the ^{14}C ages at depths of 140–343 cm have been influenced by carbon derived from reworked older sediments, which might have been eroded from exposed strata by strong winds under the cold and arid conditions of Marine Isotope Stage (MIS) 2 and then redeposited. As the remaining ^{14}C ages are conformable and appear to yield a plausible age model, these seven ages were excluded from the final age model.

The Bayesian chronology of core KY01 produced using Bacon methods (Blaauw et al., 2011, Fig. 4) yields age–depth models that give reasonable confidence for centennial-scale precision estimates (Blaauw et al., 2018). Based on the age–depth model, the extrapolated age at a depth of 7.10 m is 40 kyr BP and the sedimentation rate of the core for the interval from 0 to 7.10 m varied from 7.2 to 28.1 cm/kyr.

5.2. Grain size

The grain-size frequency distributions are variable, with modes at ~20 and ~200 μm, whereas the mean distribution exhibits a single peak centered on 10–20 μm (Fig. 5A). To determine the major factors controlling the sediment GSDs, we conducted an EMMA analysis of the grain-size dataset. Fig. 5B shows the coefficients of determination (R^2) plotted against grain size for models with 2–10 EMMA-derived end-members. The mean coefficient of determination of the grain-size classes increases with an increasing number of end-members (Fig. 5C). For the three-end-member model (R^2 mean = 0.814), $R^2 < 0.6$ for the size range >100 μm, whereas for the four-end-member model (R^2 mean = 0.967), $R^2 > 0.9$ for almost all size ranges (Fig. 5C). For five or more end-members, R^2 continues to increase, but more

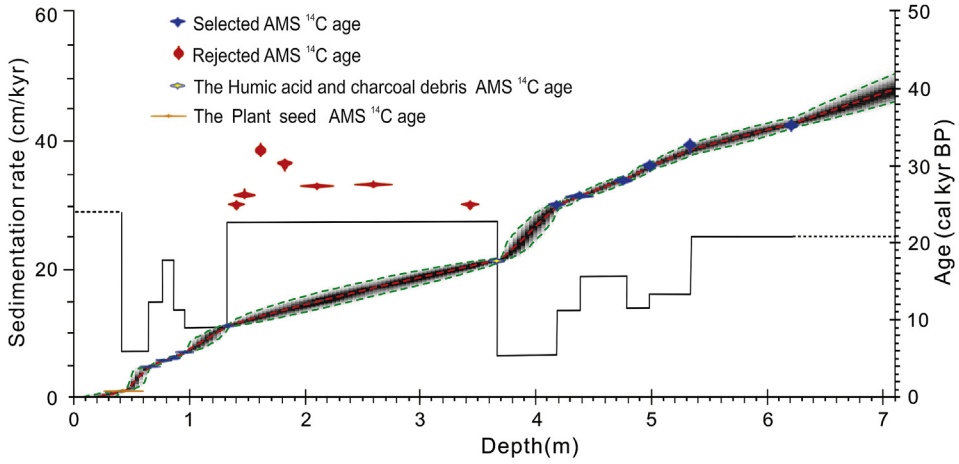

Fig. 4. Bayesian age–depth modeling for core KY01. The output graph was produced using winBacon-v2.2 (Blaauw et al., 2018). The graph shows the calibrated AMS ^{14}C ages (blue and orange) and the age–depth model (gray). Green stippled lines indicate 95% confidence intervals, and the red line denotes the single "best" model based on the weighted mean age for each depth.

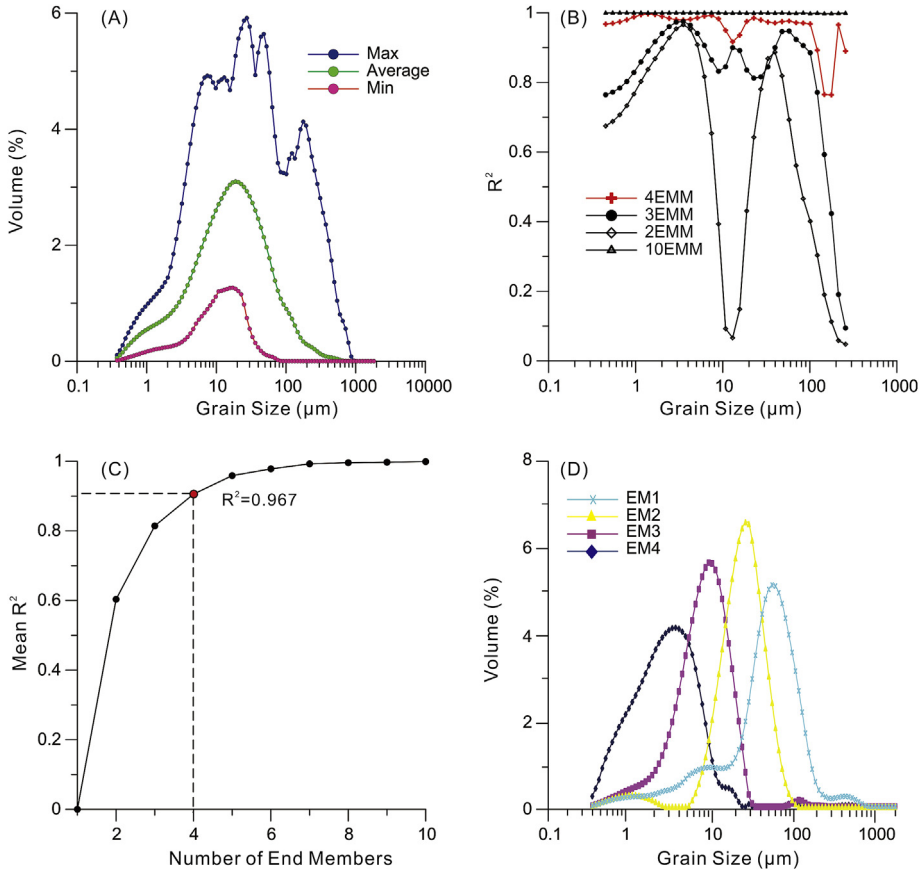

Fig. 5. End-member modeling analysis of grain-size distributions of core KY01 sediments. (A) Summary of the grain-size distributions (n = 210), including the maximum, mean value, and minimum distributions in each grain-size class. (B) Coefficients of determination (R^2) for each grain-size class of models with two to ten EMMA-derived end members. (C) Mean coefficient of determination (mean R^2) of all grain-size classes for each end-member model. The four-end-member model was selected as the best one to interpret the grain-size dataset and is highlighted by a red solid circle. (D) Grain-size distributions of the modeled end members from the selected four-end-member model.

gradually. In summary, the goodness-of-fit statistics demonstrate that the four-end-member model provides the best compromise between the number of end-members and R^2.

The modeled end-member GSDs are presented in Fig. 5D, and their respective contributions are shown in Fig. 6A–D and summarized in Table 2. All four end-members are essentially unimodal, with modal values of ~63, ~30, ~10, and ~4 μm (Table 2).

For the interval representing the past 40 kyr, the core sediments are composed primarily of silt and clay, except for coarse sand-rich layers corresponding to MIS 2 and 9–7 kyr BP (Fig. 6A–D). The contribution of the coarse fraction (modal size = 63 μm, vol. %) varies from 0% to 80.2%, with a mean of 13.2%; two prominent peaks occur in the 27.5–15.7 kyr BP and 9–7 kyr BP intervals, with the highest contribution (64.2%–80.2%) being observed for the 16.6–15.9 kyr BP interval (Fig. 6A). The contribution of the medium fraction (modal size = 30 μm, vol. %) is 0%–85.9%, with a mean of 27.1%; two prominent peaks occur during the 40–29.2 kyr BP and 26.5–13.0 kyr BP intervals, with the highest contribution (69.0%–85.9%) for the 25.2–22.6 kyr BP interval (Fig. 6B). The contribution of the fine fraction (modal size = 10 μm, vol. %) exhibits frequent oscillations between 0% and 75.4%, with a mean of 33.1%; three prominent peaks are present in the 37.3–26.5, 15.6–9.0, and 7–0 kyr BP intervals (Fig. 6C). The contribution of the finest fraction (modal size = 4 μm, vol. %) ranges from 0% to 93.9%, with a mean of 26.5%; three prominent peaks occur in the 37.4–28.0, 15.6–9.0, and 7–0 kyr BP intervals (Fig. 6D).

5.3. ln(Al/Ca) ratio

The ln (Al/Ca) ratio in core KY01 is employed a proxy for changes in climatic wetness at Lop Nur, with higher/lower values indicating wetter/drier conditions (Han et al., 1994; Li et al., 1998; Du et al., 2012; Tang et al., 2012). The values of the ratio (Supplementary Material Table) vary from −1.5 to 1.1, with a mean of −0.45. As shown in Fig. 6E, the ln (Al/Ca) ratio is generally low, with values slightly higher than average (and with fluctuations) during 39.7–27.0 kyr BP and 12.6–8.6 kyr BP; however, most of the values are below the average during MIS 2. Low values are observed during 8–6 kyr BP and since ~1.5 kyr BP.

6. Discussion

6.1. Environmental significance of grain-size end-members

Our reconstruction of past changes in dust input to sediment core KY01 is based mainly on the EMMA analysis of the sediment grain-size frequency distributions. Therefore, a reliable interpretation of the four extracted end-members is important. The grain size of lacustrine sediments from arid and semi-arid regions is controlled mainly by the grain-size composition of sediment sources as well as by fluvial and wind dynamics (Jin et al., 2000; Qiang et al., 2006). The sediments deposited at Lop Nur were transported mainly by runoff (Liu et al., 1999) derived from meltwater from snow and ice, as well as atmospheric precipitation (Luo

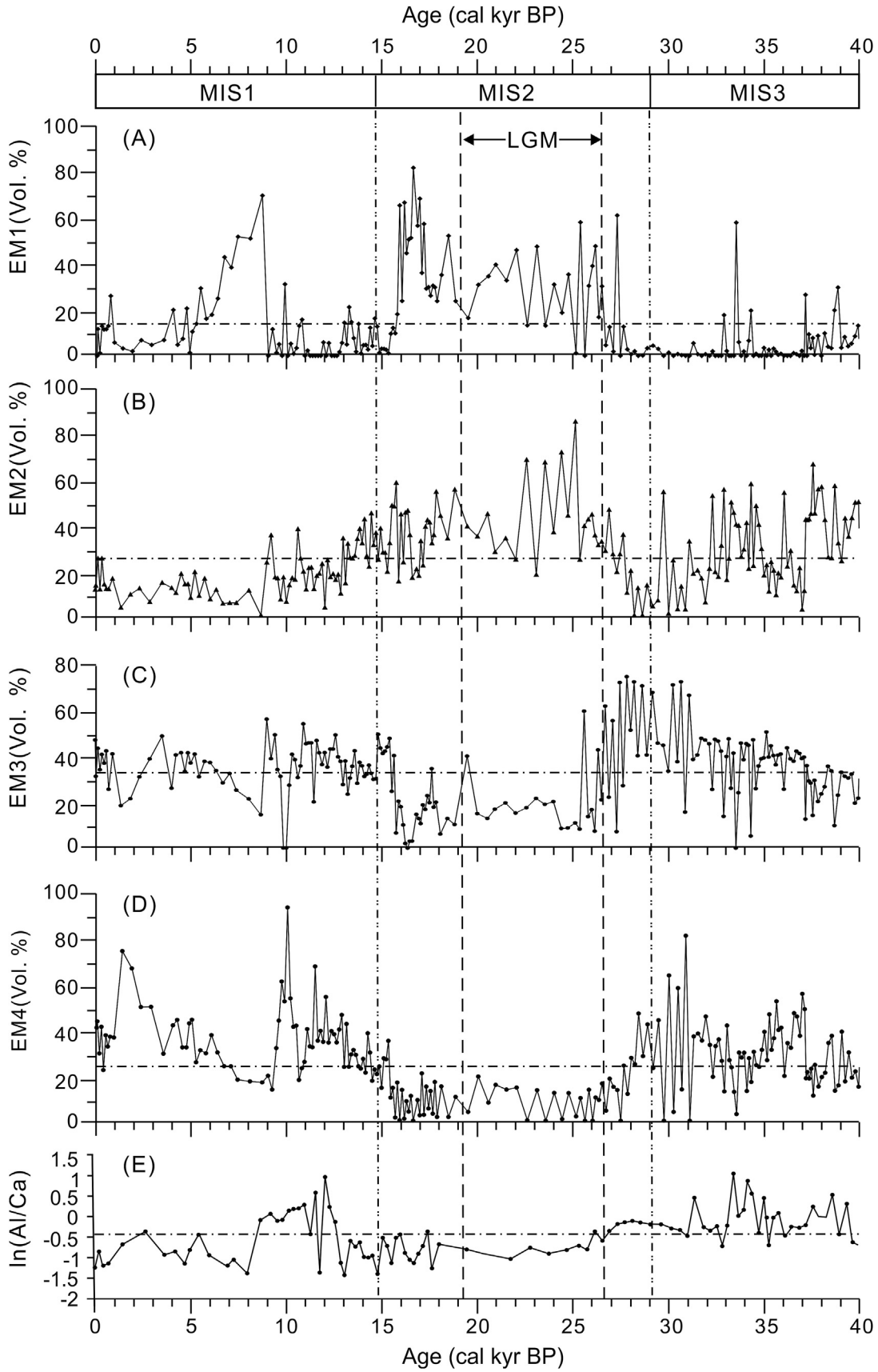

Fig. 6. Contributions of the four modeled grain-size end members to the volume of sediments in core KY01. Temporal distribution patterns of (A) EM1 Vol. %, (B) EM2 Vol. %, (C) EM3 Vol. %, and (D) EM4 Vol. % of grain size, and (E) ln (Al/Ca) ratio in core KY01 sediments from LN. The horizontal dash-dot lines in the subplots represent the average contributions of the four end-members and the ln (Al/Ca) ratio. The age boundaries of MIS 2/1 and MIS 3/2 are from Maier et al. (2018).

Table 2
Modal value, size range, minimum–maximum percentage, and average value of EMs in core KY01 from Lop Nur, Xinjiang Province, northwestern China.

Variable	EM1	EM2	EM3	EM4
Mode (μm)	63	30	10	4
Range (μm)	0.3–594	0.3–101	0.3–33	0.3–22
Min.–Max. (%)	0–80.2	0–85.9	0–75.4	0–93.9
Average (%)	13.2	27.1	33.1	26.5

et al., 2008), with the sediment transported by runoff being generally fine-grained on account of the flat terrain. The sedimentary grain size in the central parts of large lakes is mainly 2–10 μm in diameter (Yin et al., 2008), and the grain size of modern dust in northwestern China is predominantly 5–63 μm (Liu et al., 2014).

Prins et al. (2007) suggested that the dust deposited on the Chinese Loess Plateau was derived from nearby deserts. The flux of fine dust transported by high-altitude (>50 m) winds across the Chinese Loess Plateau has a modal size of 19 μm, and this flux may have been constant during the last several glacial–interglacial cycles (Prins et al., 2007). Sun et al. (2004) suggested that the fine dust component (with a modal size of ~10 μm) is transported farther downwind to more distal sites where it is eventually deposited as a background dust component. This background dust can be deposited by three mechanisms: rainfall wash-out (Rea and Hovan, 1995), attachment to larger grains (Pye, 1987), and deposition as individual particles when the wind speed decreases (Sun et al., 2004). In contrast, the coarse dust (with modal sizes of ~63 and ~40 μm) transported by low-level (<50 m) winds varies substantially with climatic conditions; such dust is supplied mainly from more proximal sources during major dust outbreaks in spring–summer (Prins et al., 2007).

Based on the above, we interpret the four grain-size end-members identified in the sediments of core KY01 as follows. 1) A coarse fraction (EM1, modal size 63 μm) probably reflects the dust supplied during major dust outbreaks and possibly transported by saltation (Prins et al., 2007). 2) A medium fraction (EM2, modal size 30 μm) represents dust transported by low-level (<50 m) winds during major dust outbreaks (Prins et al., 2007). The sum of the fluxes of the low-altitude wind-blown dust is a good approximation of the flux from the dust source (Vriend et al., 2011). Therefore, the sum of the two coarse-grained dust fractions (EM1 + EM2) is used here as a proxy for the intensity of dust storm activity over the dust source region, whereas the ratio of EM1/(EM1 + EM2) is used to represent the capacity of low-level winds to transport dust (Stuut et al., 2002; Qiang et al., 2010). 3) A fine fraction (EM3, modal size 10 μm) possibly represents the background dust aerosol, which is commonly carried by high-altitude westerly air streams (Sun et al., 2004; Prins et al., 2007). The fine fraction (EM3) is used here to represent the background dust load of the atmosphere, which is transported mainly by high-altitude westerly airstreams. The modal grain sizes of the coarse and fine dust fractions are considered to provide an estimate of the intensities of the low-altitude northwesterly and high-altitude westerly airstreams, respectively (Sun et al., 2004; Prins et al., 2007). 4) The finest fraction (EM4, modal size 4 μm) reflects fluctuations in runoff and the related volume of the Lop Nur paleolake (Peng et al., 2005).

6.2. Alternating arid and wet conditions at Lop Nur since 40 kyr BP

Geochemical proxies of sediments have been successfully applied to the paleoenvironmental reconstruction of arid regions (Jia et al., 2012; Cheng et al., 2013), although their correlation at large spatial scales can be difficult because geochemical elements and their ratios are strongly dependent on local environmental conditions (Cheng et al., 2013). For example, Al is stable during chemical weathering and is readily transported to lakes by runoff as part of the clastic sediment component (Han et al., 1994; Du et al., 2012). Ca, in contrast, is readily leached and transported, usually as Ca^{2+} or a Ca-bearing colloid. In wet climates, in which Al is readily transported to lakes by runoff and deposited, Ca might not be precipitated owing to the freshwater conditions and lowered lake-water pH (Han et al., 1994). In contrast, during the dry season the reduced runoff restricts the transport of aluminiferous clasts (Han et al., 1994; Du et al., 2012), whereas Ca can still be transported to lakes and precipitated as evaporites (Han et al., 1994; Li et al., 1998; Du et al., 2012; Tang et al., 2012). The ln (Al/Ca) ratio can thus be used as a proxy for the occurrence of wet/dry conditions in areas with saline lakes.

Previous studies have concluded that the environment of Lop Nur changed substantially during the late Pleistocene, with the paleolake experiencing several periods of expansion and contraction in response to alternating arid and wet conditions (Yan et al., 1998; Wang et al., 2001; 2006; Xia et al., 2007). At 40–29 kyr BP, lacustrine strata were widely distributed in the central and southern parts of the Taklamakan Desert, suggesting that the local climate was generally wet (Yang et al., 2006). Lop Nur might have been weakly affected by the Heinrich 4 (H4) cold event, as the ln (Al/Ca) ratio was higher than average, indicating that the climate was wet during this event. Subsequently, the ln (Al/Ca) ratio increased with small-amplitude fluctuations, indicating that the climate became wetter overall (Fig. 7A). Pollen records from lacustrine sediments on the Tibetan Plateau suggest that local precipitation during MIS 3 was much higher than that of the modern climate (by 40%–100%) because of the enhanced Indian summer monsoon (Shi et al., 2001). The level of Gahai Lake in the Qaidam Basin was relatively high (Fan et al., 2010) until ~25 kyr BP, when the climate became arid (Chen and Bowler, 1986). A sedimentary sequence from the western part of the Chinese Loess Plateau, which records alternating lacustrine and wetland environments, also indicates relatively wet conditions during MIS 3, possibly related to local summer and winter solar insolation (Feng et al., 2007). Yang et al. (2011) suggested that during MIS 3, particularly at ~30 kyr BP, the relatively wet climate of the Taklamakan Desert and the Qaidam Basin was related to an enhancement of the Arctic High and wind stress associated with the northwesterly wind. Lop Nur, adjacent to the western Taklamakan Desert, was located in a relatively humid environment and had dense vegetation cover at this time (Yang and Scuderi, 2010; Chang et al., 2012).

Lake levels track changes in the ratio of precipitation to evaporation and can therefore be used to infer moisture transport (Yu et al., 2003; Bian et al., 2010). From 40 to ~29 kyr BP the contribution of alluvial mud (EM4) was generally high (Fig. 7B), as also indicated by the high ln (Al/Ca) ratio (Fig. 7A), suggesting relatively wet conditions. This finding is consistent with lacustrine sedimentary records from other parts of western China (Chen and Bowler, 1986; Shi et al., 2001; Feng et al., 2007; Fan et al., 2010).

MIS 2 (29–14.7 kyr BP, Maier et al., 2018) was a mainly cold interval with low sea level, when ice sheets occupied large areas of Europe and North America (Mix et al., 2001; Clark et al., 2009), causing a reorganization of major atmospheric and hydrological systems in the Northern Hemisphere (Shakun and Carlson, 2009). The Last Glacial Maximum (LGM, 26.5–19.2 kyr BP; Clark et al., 2009) was characterized by the coldest climatic conditions, the lowest sea level, and the largest terrestrial ice volumes in Europe and North America during the Last Glacial (Mix et al., 2001; Clark et al., 2009). During MIS 2, the ln (Al/Ca) ratio in core KY01 was relatively low, generally less than average, especially during the

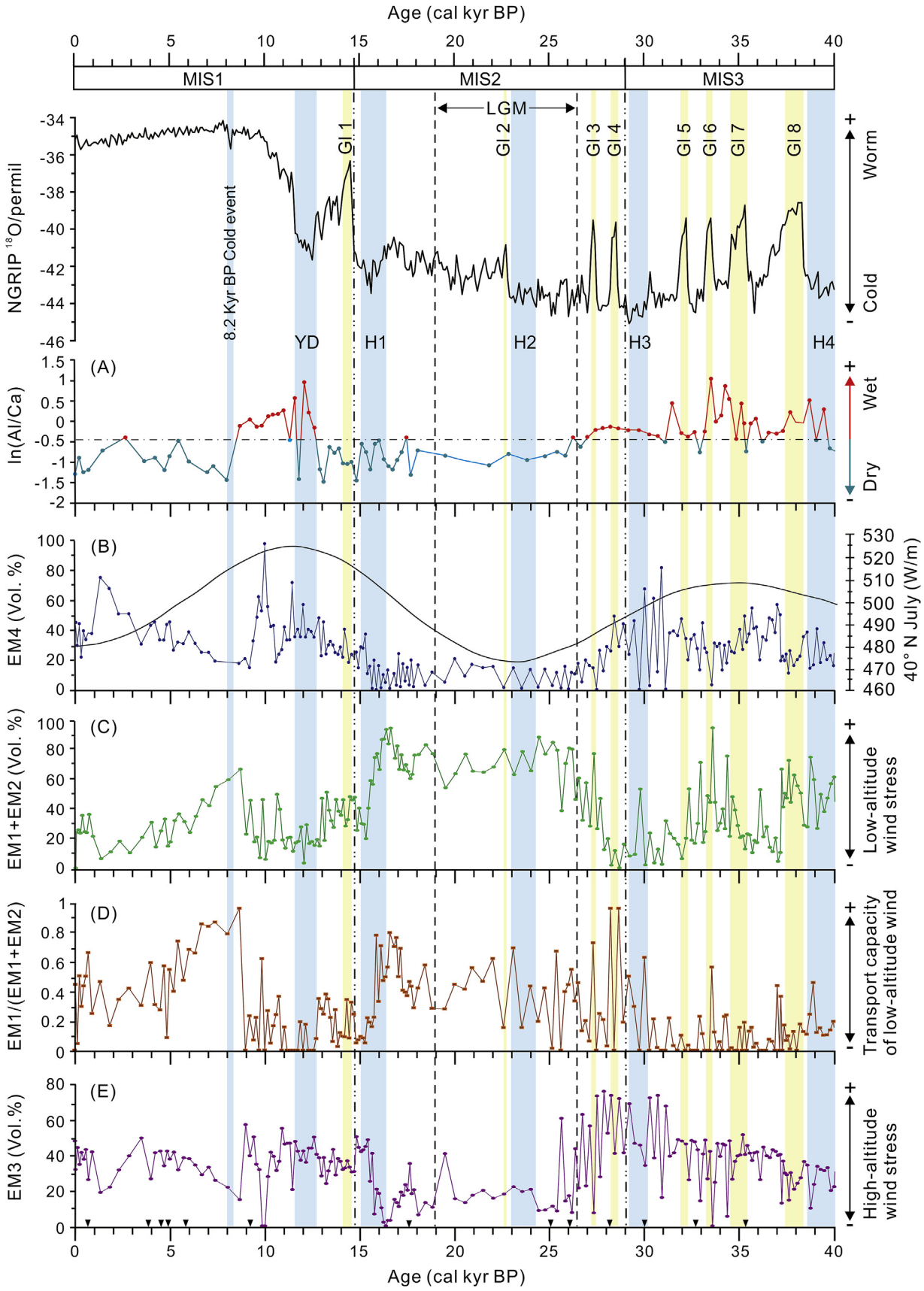

Fig. 7. Comparison of the grain-size end-members and ln (Al/Ca) ratio of the studied core KY01 with the NGRIP δ^{18}O record (North Greenland Ice-Core Project Members, 2004). (A)–(E) ln (Al/Ca), alluvial mud (EM4), coarse-grained dust components (EM1 + EM2), EM1/(EM1 + EM2), and fine-grained dust component (EM3), respectively. In (A) the horizontal dash–dot line represents the average ln (Al/Ca) value, and red and blue sections of the line denote values above and below the average ln (Al/Ca) ratio, respectively. Inverted

LGM, and this indicates an extremely cold and dry climate. Thus, the variations in the ln (Al/Ca) ratio at Lop Nur do not support the inference of an extremely humid LGM in central Asia, challenging the proposition of cold–moist (glacial) and warm–dry (interglacial) patterns of late Quaternary environmental change in central Asia (Ma et al., 2004; Luo et al., 2009). The regional vegetation around Lake Balikun during the LGM was dominated by desert vegetation, with typical desert–steppe and/or desert taxa, reflecting the progressive aridification of the eastern Tien Shan in northwestern China (An et al., 2013).

During MIS 2 the contribution of alluvial mud (EM4) decreased abruptly, with most values being below average, indicating a reduced influx of meltwater from snow and ice and an intensified Arctic High and northwesterly wind (Nagashima et al., 2011; Martrat et al., 2014; Oster et al., 2015). These changes would have intensified the already dry climate. During the H1 cold event, in particular, Lop Nur experienced a cold climate, and the contribution of alluvial mud (EM4) decreased to its lowest level of the entire sequence, possibly because meltwater input ceased almost completely (Fig. 7B). At this time, the Lop Nur paleolake might have dried up almost completely. Prokopenko et al. (2005) demonstrated the occurrence of similarly dry conditions in Mongolia during the LGM, when very low water levels occurred at Hovsgol Lake. During MIS 2, Balikun Lake shrank to its minimum level, and the surrounding area recorded a minimum in vegetation cover (An et al., 2013). Thus, extremely cold and dry conditions prevailed in northwestern China during 17.0–15.2 cal kyr BP, the interval corresponding to the H1 event (Zhao et al., 2015).

Subsequently, the contribution of alluvial mud (grain-size component EM4) increased continuously in core KY01 and the volume of the paleolake started to expand during the Greenland interstadial (GI) 1, when local vegetation flourished (Lehmkuhl and Haselein, 2000; Chang et al., 2012; Dong et al., 2013; Zhao et al., 2015). During the early part of MIS 1 (14.7–12.8 kyr BP) the ln (Al/Ca) ratio was generally lower than the average, indicating a relatively cold and dry climate. During 11.8–12.8 kyr BP the relatively cold climate was interrupted by an abrupt increase in moist conditions during the cold Younger Dryas (YD). A previous study of the sulfate and chloride contents of the lacustrine sediments of Lop Nur also suggested the occurrence of relatively moist climatic conditions during the YD (Hua et al., 2009), in good agreement with the increased ln (Al/Ca) ratio in core KY01 (Fig. 7A). High ln (Al/Ca) ratios during 11.8–9 kyr BP indicate relatively wet conditions at Lop Nur during the early Holocene. In addition, the input of alluvial mud (EM4) increased gradually, consistent with the increased ln (Al/Ca) ratio in core KY01 and with the gradual increase in summer insolation (Laskar et al., 2004) (Fig. 7A and B).

During 9–7 kyr BP the ln (Al/Ca) ratio again shows a rapid decline that might reflect the 8.2 kyr BP cold event recorded in the $\delta^{18}O$ record of the NGRIP Greenland ice core (North Greenland Ice Core Project Members, 2004), and hence the return of a cold and dry climate. At the same time, a marked decrease in the contribution of the EM4 component suggests a decrease in runoff at Lop Nur, possibly caused by reduced meltwater input in response to lower temperatures.

From ~7.0 to ~1.5 kyr BP the ln (Al/Ca) ratio increased gradually, with low-amplitude fluctuations, indicating that the climatic conditions remained moderately arid following the 8.2 kyr BP cold event, before gradually becoming wetter between ~3.5 and ~1.5 kyr BP. After ~1.5 kyr BP the ln (Al/Ca) ratio decreased to below average, indicating the return of arid climatic conditions. The alluvial mud component (EM4), reflecting runoff, generally increased from ~7.0 to ~1.5 kyr BP, reflecting the further expansion of the paleolake under progressively wetter conditions. Lacustrine sedimentary records from other parts of Xinjiang, northwestern China, indicate a similar climate that represents the Holocene Climatic Optimum. For example, multi-proxy analyses of core BST04H from Bosten Lake (Fig. 1A) suggest that the water depth of the lake reached a maximum at ~6 kyr BP (Chen et al., 2006), demonstrating an increase in precipitation (Zhong et al., 2005). The occurrence of climatic fluctuations at ~1.5 kyr BP is indicated by an optically stimulated luminescence (OSL) age of 2320 ± 180 yr for the boundary between lacustrine sediments and overlying dust deposits from the southern margin of the Taklamakan Desert (Fig. 1A; Yang et al., 2006). After ~1.5 kyr BP the ln (Al/Ca) ratio decreased and the contribution of EM4 rapidly declined (Fig. 7A and B), suggesting a decrease in the area of the paleolake and hence the return of an arid climate and the deterioration of the environment in Lop Nur.

6.3. Changes in dust activity since 40 kyr BP

Dust activity is controlled mainly by three factors: dust source, weather conditions, and roughness of the terrain along the wind path (Liu et al., 2005; Lv et al., 2011; Xu et al., 2015). Dust particles can be transported by creep, saltation, and in suspension. Aggregates or particles of <0.1 mm in diameter are generally suspended above the surface, whereas particles and/or aggregates of 0.1–2.0 mm in diameter move by creep and saltation across the surface (Hagen et al., 1999).

From 40 to 29 kyr BP, dust storm activity at Lop Nur gradually decreased, and there was only a moderate contribution of the EM1 + EM2 components during 32–30, 14.9–9.0, and 7.0 to ~1.5 kyr BP (Fig. 7C). However, the input of coarse dust (EM1 + EM2) increased during the H4 cold event, and during intervals between the warm interstadials of GI 8 and GI 7, and GI 7 and GI 6 (Fig. 7C). The increased coarse dust inputs during the intervals between warm interstadials might have been caused by decreased atmospheric temperature (North Greenland Ice Core Project Members, 2004), which reduced the influx of meltwater from snow and ice, causing the paleolake to shrink and enabling the coarse dust carried by low-level winds to reach the center of the lake (Qiang et al., 2010). During the same period, the contribution of fine dust (EM3) gradually increased, with superimposed small-amplitude fluctuations. After the H3 cold event, the contribution of EM3 again increased rapidly (Fig. 7E). The fine dust was deposited partly in the form of silt-sized aggregates and as attachments to large grains during dust storms, although some fine particles might have been deposited as discrete grains during quiescent periods by rainfall scavenging (Sun et al., 2004; Qiang et al., 2010). The contribution of the EM3 component increased during warm intervals, probably because of an enhanced intensity of the high-level westerly airstream and increased precipitation (Sun et al., 2004; Prins et al., 2007; Qiang et al., 2010).

During MIS 2, summer insolation at 40°N decreased (Laskar et al., 2004, Fig. 7B) and the climate of the Tarim Basin became extremely arid (Yang et al., 2006). In response to these climatic changes, the vegetation coverage was reduced, the Taklamakan Desert expanded (Lehmkuhl and Haselein, 2000; Chang et al., 2012; Dong et al., 2013), and sandstorm activity intensified. Furthermore,

triangles at the base of (F) represent selected AMS ^{14}C ages (Fig. 4; Table 1). Light-blue vertical bars represent the 8.2 kyr cold event, the Younger Dryas (YD), and Heinrich events (H1–H4). Warm interstadials (GI 1 to GI 8) are indicated by light-yellow vertical bars. The ages of the YD, H1–H4, and GI 1 to GI 8 are from Blockley et al. (2012). The Last Glacial Maximum (LGM, 26.5–19.2 kyr; Clark et al., 2009) is indicated by the interval between the two vertical dashed lines. July insolation at 40°N is from Laskar et al. (2004) and the ages of the MIS 2/1 and MIS 3/2 boundaries are from Maier et al. (2018).

the contribution of coarse-grained dust components (EM1 + EM2) (Fig. 7C) exhibited a rapid increase during early MIS 2 and subsequently remained at a high level, possibly because of meltwater reduction together with an intensified Arctic High and enhanced northwesterly wind (Nagashima et al., 2011; Martrat et al., 2014; Oster et al., 2015), which triggered intense sandstorm activity. Atmospheric circulation simulations suggest that the northwesterly wind was strengthened during the LGM (Kutzbach, 1980), and the expanded global ice volume enhanced the Asian winter monsoon by strengthening the Mongolian High (Ding et al., 1995). The mean annual temperature during the LGM was lower than that of the present day in arid western China (Liu et al., 2002; Yang et al., 2002) as a result of decreased high-latitude summer insolation and changes in other boundary conditions (Clark et al., 2009). The presence of mountain glaciers (Takeuchi et al., 2014) and their limited meltwater contributions might have resulted in a contemporaneous low-stand in lake level. The high contribution of coarse-grained dust components (EM1 + EM2) indicates that low-level winds were extremely strong, as suggested by the EM1/(EM1 + EM2) ratio (Fig. 7C and D). Associated with the expansion of the Taklamakan Desert, strong dust storms occurred frequently at Lop Nur during the LGM (Lehmkuhl and Haselein, 2000; Li et al., 2010; Chang et al., 2012; Dong et al., 2013; Lu and Guo, 2015).

During the H1 cold interval the low-altitude wind stress was strong, as reflected by the ln (Al/Ca) ratios, which indicate the occurrence of minimum runoff at Lop Nur (Fig. 7A and B). At the same time, the greatly reduced vegetation cover enabled an influx of large amounts of dust into the Lop Nur paleolake, and Balikun Lake in the eastern Tien Shan, western China, was reduced to its minimum extent (Zhao et al., 2015). Decreasing sea-surface temperature and salinity in the North Atlantic during the H1 cold event resulted in an abundant supply of ice and ice-rafted debris to the ocean (Heinrich, 1988; Hemming, 2004). During the early part of MIS 1 (14.7–9.0 kyr BP) the supply of coarse dust to the Lop Nur paleolake decreased abruptly, as indicated by low values of EM1/(EM1 + EM2) (Fig. 7D), possibly because of the combined effects of the expanded area of the paleolake and increased vegetation coverage and atmospheric humidity (Yang et al., 2009). During the warm interstadial GI 1 the contribution of coarse dust (EM1 + EM2) decreased and that of fine dust (EM3) increased (Fig. 7C and E). At that time, the paleolake expanded and the local vegetation flourished (Lehmkuhl and Haselein, 2000; Chang et al., 2012; Dong et al., 2013), and the low-level wind stress and associated sandstorm activity were therefore greatly reduced (Lv et al., 2011; Li et al., 2014). The trend of rapidly increasing temperature was interrupted by the YD cold event (Ma et al., 2012), when the contributions of the coarse-grained dust components (EM1 + EM2) decreased substantially (Fig. 7C), associated with an expanded Lop Nur paleolake, when only a small amount of coarse dust (Fig. 7C) could reach the lake center.

From 9 to 7 kyr BP the content of coarse-grained dust (EM1 + EM2) and the ratio of EM1/(EM1 + EM2) increased rapidly (Fig. 7C and D), possibly because of outbreaks of very strong dust storms. In addition, the paleolake dried up almost completely, enabling coarse-grained dust to reach the center. The low-level wind stress was as strong as that during the H1 cold interval (Fig. 7C), and the climate was extremely arid (Fig. 7A and B), meaning that the intermittent suspended dust could not easily reach the lake center (Fig. 7E). Consequently, there were abrupt fluctuations in the four grain-size end-member contributions (EM1–EM4) during this interval, which spans the 8.2 kyr BP cold event. During this cold event, which was of global scale (Alley and Agustsdottir, 2005; Wang, 2008), most parts of the Northern Hemisphere were cold and dry, especially Greenland (North Greenland Ice Core Project Members, 2004), where the atmospheric temperature decreased by ~6 °C (Kobashi et al., 2007; Thomas et al., 2007). Several yellowish silt layers (0.3–0.8 cm thick) are evident in outcrops of Quaternary lacustrine sediments at Lop Nur. The frequency of these layers peaked at ~8.2 kyr BP, which indicates the occurrence of cold and windy conditions (Liu et al., 2003); similar climate changes are recorded elsewhere in Xinjiang (Yao et al., 1992; Zhong et al., 2005; Yang et al., 2015). During ~8.2 kyr BP, the meltwater supply to Lop Nur might have been reduced as a result of the expansion of mountain glaciers and ice sheets on the Tibetan Plateau (Jiao et al., 2000).

From 7.0 to ~3.5 kyr BP, dust storm activity and low-altitude wind stress gradually decreased (Fig. 7C and D), whereas high-altitude wind stress increased, possibly because of an expansion of the lake area and reduced low-level wind stress (Chen et al., 2006). The low-level wind (northwesterly) was the likely transport agent for all three dust components. In addition, recent research near Alaer City, in the northwestern Tarim Basin, indicates that fine dust is derived from the direct emission of fine particles during the abrasion of coarser particles, either airborne or on the ground surface (Pi et al., 2017, Fig. 1).

From ~3.5 to ~1.5 kyr BP the fine dust component was reduced, indicating a reduction in both the strength of the high-level westerly airstream and precipitation (Sun et al., 2004; Prins et al., 2007; Qiang et al., 2010). In addition, the contributions of the coarsest dust (EM1) and coarser dust (EM2) were lower, as was the value of the EM1/(EM1 + EM2) ratio, suggesting that dust storms were persistently weak. It is likely that part of the fine-grained EM3 component deposited in the lake center was transported in the form of aggregates or by adhering to larger particles. After ~1.5 kyr BP there was an increase in the input of coarse dust associated with dust storm activity, indicating that low-level wind stress had again increased (Fig. 7C and D).

7. Conclusions

We used AMS ^{14}C dating, analyses of sediment lithology, ln (Al/Ca) ratios, and four grain-size end-members extracted using EMMA of grain-size data to study the sediments of core KY01 from the Lop Nur paleolake, Xinjiang Province, northwestern China. The results enable us to reconstruct changes in aridity and dust activity over the past 40 kyr. Our principal findings are as follows.

1. The ln (Al/Ca) ratio and grain-size component EM4, which reflect variations in runoff, are effective indicators of local wetness conditions. During 40.0–26.5, 12.8–9.0, and ~3.5–1.5 kyr BP the Tarim Basin generally experienced wet climatic conditions, whereas extremely arid conditions occurred during the LGM, H1, and YD intervals and around the time of the 8.2 kyr BP cold interval.
2. The input of coarse dust (grain-size components EM1 + EM2) to the Lop Nur paleolake exhibits a decreasing trend with frequent fluctuation during mid–late MIS 3, caused mainly by an expansion of the area of the paleolake and low low-level wind stress. During MIS 2, especially during the LGM and H1 cold intervals, the climate of Lop Nur deteriorated significantly: the climate was arid, the low-level winds were strong, and dust storms were frequent. During early MIS 1 the dust contributed by sandstorms gradually decreased, and this input increased only slightly during the YD cold interval. During 9–7 kyr BP the strength of low-level winds and dust storm inputs increased again, possibly in response to the 8.2 kyr BP cold event; however, both decreased in the interval from 7.0 to ~1.5 kyr BP. After ~1.5 kyr BP the coarse dust input increased, with fluctuations. We conclude that dust storm activity at Lop Nor since 40 kyr BP

has been driven mainly by cold events in the high-latitude Northern Hemisphere and by low-level northwesterly winds.

3. At Lop Nur the input of fine dust (grain-size component EM3), which is the atmospheric background dust component, increased mainly during MIS 3 and the Holocene, forced by variations in the high-altitude westerly air stream. This conclusion is significant for identifying the mechanisms responsible for dust transport and deposition, as reflected in lacustrine sedimentary records, as well as for improving our understanding of the environmental evolution of northwestern China.

Acknowledgments

We thank two anonymous reviewers for their thoughtful suggestions that helped to significantly improve an earlier version of this manuscript. We also thank Dr. Li Wu of the State Key Laboratory of Marine Geology, Tongji University, for his help with computing and with deciphering the grain-size end-members. This study was supported financially by the Geological Investigation Project of China Geological Survey [Grant Nos. 1212011120044, 12120113006200, and DD20160060] and the National Natural Science Foundation of China [Grant No. 41572351].

Appendix A. Supplementary data

Supplementary data to this article can be found online at https://doi.org/10.1016/j.quascirev.2019.03.023.

References

Alley, R.B., Agustsdottir, A.M., 2005. The 8k event: cause and consequences of a major Holocene abrupt climate change. Quat. Sci. Rev. 24, 1123–1149.
An, C.B., Tao, S.C., Zhao, J.J., Chen, F.H., Lv, Y.B., Dong, W.M., Zhao, Y.T., Wang, Z.L., 2013. Late Quaternary (30.7–9.0 cal ka BP) vegetation history in Central Asia inferred from pollen records of Lake Balikun, northwest China. J. Paleolimnol. 49, 145–154.
Aravena, R., 1992. Carbon isotope composition of lake sediments in relation to lake productivity and radiocarbon dating. Quat. Res. (Duluth) 37, 333–345.
Bian, D., Bian, B., Wang, C.Y., Chen, T., 2010. The response of water level of Selin Co to climate change during 1975–2008. Acta Geograph. Sin. 65, 313–319 (in Chinese with English abstract).
Blaauw, M., Christen, J.A., 2011. Flexible paleoclimate age-depth models using an autoregressive gamma process. Bayesian Anal 3, 457–474.
Blaauw, M., Christen, J.A., Bennett, K.D., Reimer, P.J., 2018. Double the dates and go for Bayes—impacts of model choice, dating density and quality on chronologies. Quat. Sci. Rev. 188, 58–66.
Blockley, S.P.E., Lane, C.S., Hardiman, M., Rasmussen, S.O., Seierstad, I.K., Steffensen, J.P., Svensson, A., Lotter, A.F., Turney, C.S.M., Ramsey, C.B., INTIMATE members, 2012. Synchronisation of palaeoenvironmental records over the last 60,000 years, and an extended INTIMATE1 event stratigraphy to 48,000 b2k. Quat. Sci. Rev. 36, 2–10.
Chang, Z.F., Wang, Y.L., Han, F.G., Zhong, S.N., 2012. Relationship between frequency of sandstorms and air humidity as well as plant phenology: a case study from the Minqin desert area. Acta Ecol. Sin. 32, 1378–1386 (in Chinese with English abstract).
Chen, K., Bowler, J.M., 1986. Late Pleistocene evolution of salt lakes in the Qaidam Basin, qinghai province, China. Palaeogeogr. Palaeoclimatol. Palaeoecol. 54, 87–104.
Chen, J.A., Wan, G.J., Tang, D.G., 2000. A sediment grain size and isotope record of recent climate change in Erhai. Prog. Nat. Sci. 10, 253–259 (in Chinese).
Chen, F.H., Zhu, Y., Li, J.J., Shi, Q., Jin, L.Y., Wunemann, B., 2001. A lacustrine sedimentary record of rapid millennial–centennial variability of the Quaternary summer monsoon from the Minqin Basin. Chin. Sci. Bull. 46, 1414–1419 (in Chinese).
Chen, F.H., Huang, X.Z., Yang, M.L., Yang, X.L., Fan, Y.X., Zhao, H., 2006. Westerly dominated Holocene climate model in arid central Asia—case study on Bosten lake Xinjiang China. Quat. Sci. 26, 881–887 (in Chinese with English abstract).
Cheng, H., An, Z.S., Wu, F., Jin, Z.D., Liu, W.G., Song, Y.G., 2013. A Rb/Sr record of the weathering response to environmental changes in westerly winds across the Tarim Basin in the late Miocene to the early Pleistocene. Palaeogeogr. Palaeoclimatol. Palaeoecol. 386, 364–373.
Clark, P.U., Dyke, A.S., Shakun, J.D., Carlson, A.E., Clark, J., Wohlfarth, B., Mitrovica, J.X., Hostetler, S.W., McCabe, A.M., 2009. The last glacial maximum. Science 325, 710–714.
Dietze, E., Hartmann, K., Diekmann, B., IJmker, J., Lehmkuhl, F., Opitz, S., Stauch, G., Wünnemann, B., Borchers, A., 2012. An end-member algorithm for deciphering modern detrital processes from lake sediments of Lake Donggi Cona, NE Tibetan Plateau. China. Sediment. Geol. 243–244, 169–180.
Ding, Z.L., Liu, T.S., Rutter, N.W., Yu, Z.W., Guo, Z.T., Zhu, R.X., 1995. Ice-volume forcing of East Asian winter monsoon variations in the past 800,000 years. Quat. Res. (Duluth) 44, 149–159.
Dong, Z.B., Lv, P., Qian, G.Q., Xia, X.C., Zhao, Y.J., Mu, G.J., 2012. Research progress in China's Lop Nur. Earth Sci. Rev. 111, 142–153.
Dong, L.N., Lu, H.Y., Wang, X.Y., Ge, S.F., Wang, X.Y., Zhao, C.F., Xu, Z.W., Zeng, L., Zhu, F.Y., 2013. A tentative reconstruction of the border migration of Xinjiang deserts during the last glacial maximum and Holocene optimum. Quat. Sci. 33, 398–400 (in Chinese with English abstract).
Du, C., Zhang, B., Zhang, S.T., Sun, Q.S., Li, C., 2012. Application and principle of element geochemistry in the evolution of lake sedimentary environment. Geol. Resour. 21, 487–492 (in Chinese with English abstract).
Fan, Q.S., Lai, Z.P., Long, H., Sun, Y.J., Liu, X.J., 2010. OSL chronology for lacustrine sediments recording high stands of Gahai Lake in Qaidam Basin, northeastern Qinghai–Tibetan Plateau. Quat. Geochronol. 5, 223–227.
Fan, Q.S., Ma, H.Z., Ma, Z.B., Wei, H.C., Han, F.Q., 2014. An assessment and comparison of ^{230}Th and AMS ^{14}C ages for lacustrine sediments from Qarhan Salt Lake area in arid western China. Environ. Earth Sci. 71, 1227–1237.
Feng, Z.D., Tang, L.Y., Ma, Y.Z., Zhai, Z.X., Wu, H.N., 2007. Vegetation variations and associated environmental changes during marine isotope stage 3 in the western part of the Chinese Loess Plateau. Palaeogeogr. Palaeoclimatol. Palaeoecol. 246, 278–291.
Hagen, L.J., Wagner, L.E., Skidmore, E.L., 1999. Analytical solutions and sensitivity analysis for sediment transport in WEPS. Trans. Am. Soc. Agric. Eng. 42, 1715–1721.
Han, S.T., Li, Z.Z., 1994. The accumulating regulation of deposit geochemistry of Balikun Lake, Xinjiang. Oceanol. Limnol. Sinica 25, 429–437 (in Chinese with English abstract).
Hateren, J.A.V., Prins, M.A., Balen, R.T.V., 2017. On the genetically meaningful decomposition of grain–size distributions: a comparison of different end-member modelling algorithms. Sediment. Geol. 202, 409–424.
He, Q., Yang, X.H., Ai, L., 2011. Observation of dust emission by wind erosion in Taklamakan Desert: field experiment and preliminary report. Chin. Desert 31, 315–322 (in Chinese with English abstract).
Heinrich, H., 1988. Origin and consequences of cyclic ice rafting in the northeast Atlantic Ocean during the past 130,000 years. Quat. Res. (Duluth) 29, 142–152.
Hemming, S.R., 2004. Heinrich events: massive late Pleistocene detritus layers of the North Atlantic and their global climate imprint. Rev. Geophys. 42, 1–43.
Heslop, D., Von Dobeneck, T., Höcker, M., 2007. Using non-negative matrix factorization in the "unmixing" of diffuse reflectance spectra. Mar. Geol. 241, 63–78.
Hou, J.Z., D'Andrea, W.J., Liu, Z.H., 2012. The influence of ^{14}C reservoir age on interpretation of paleolimnological records from the Tibetan Plateau. Quat. Sci. Rev. 48, 67–79.
Hua, Y.S., Jiang, P.A., Wu, H.Q., Zhong, J.P., Ma, L.C., Li, B.G., 2009. The sedimentary characteristics of L07-10 profile and its environmental indicator in Lop Nur "Great Ear" Area. J. Xinjiang Agric. Univ. 32, 36–39 (in Chinese with English abstract).
Jäkel, D., Grunert, J., 2003. Die wüsten zentralasiens. Petermanns Geogr. Mittl. 147, 26–33.
Jia, H.J., Qin, X.G., Liu, J.Q., 2012. Environmental changes recorded by major elements in Loulan Stupa Section during early–middle Holocene. J. Earth Sci. 23, 155–160.
Jiao, K.Q., Yao, T.D., Li, S.J., 2000. Evolution of glaciers and environment in the West Kunlun Mountains during the past 32 ka. J. Glaciol. Geocryol. 22, 250–256 (in Chinese with English abstract).
Jin, Z.D., Wang, S.M., Shen, J., Zhang, E.L., Wang, J., Chen, Y., Chen, S.T., 2000. Dust-storm events in Daihai Lake area, Inner Mongolia during the past 400 years: evidence from grain-size analysis of lake sediments. J. Lake Sci. 12, 193–198 (in Chinese with English abstract).
Jonkers, L., Prins, M.A., Brummer, G.J.A., Konert, M., Lougheed, B.C., 2009. Experimental insights into laser diffraction particle sizing of fine-grained sediments for use in palaeoceanography. Sedimentology 56, 2192–2206.
Kelts, K., Ding, Z.L., 1992. Lacustrine deposit-information base in the past. Quat. Sci. 2, 138–143 (in Chinese).
Kobashi, T., Severinghaus, J.P., Brook, E.J., Barnola, J.M., Grachev, A.M., 2007. Precise timing and characterization of abrupt climate change 8200 years ago from air trapped in polar ice. Quat. Sci. Rev. 26, 1212–1222.
Kutzbach, J.E., 1980. Estimates of past climate at Paleolake Chad, North Africa, based on a hydrological and energy-balance model. Quat. Res. (Duluth) 14, 210–223.
Laskar, J., Robutel, P., Joutel, F., Gastireau, M., Corria, A.C.M., Levrard, B., 2004. A long term numerical solution for the insolation quantities of the Earth. Astron. Astrophys. 428, 261–285.
Lehmkuhl, F., Haselein, F., 2000. Quaternary paleoenvironmental change on the Tibetan Plateau and adjacent areas (Western China and Western Mongolia). Quat. Int. 65/66, 121–145.
Li, B.X., Cai, B.,Q., Liang, Q.S., 1998. Sedimentary characteristics of aydingkol Lake in turpan basin. Chin. Sci. Bull. 8, 608–610 (in Chinese with English abstract).
Li, J.C., Dong, Z.B., 2010. Research progress and prospect of dustfall research. J. Arid Land Resour. Environ. 24, 102–109 (in Chinese with English abstract).
Li, Y.Y., Zhang, Q., Chen, Y., Hu, X.C., 2014. Vertical structure of atmosphere boundary layer during wind-sandstorm process over sandstorm source in arid area of

northwest China. J. Desert Res. 34, 206–214 (in Chinese with English abstract).
Liu, C.L., Wang, M.L., Jiao, P.C., 1999. Hydrogen, oxygen, strontium and sulfur isotopic geochemistry and potash-forming material sources of Lop Salt Lake, Xinjiang. Miner. Deposita 18, 268–275 (in Chinese with English abstract).
Liu, C.L., Wang, M.L., Jiao, P.C., Li, S.D., Chen, Y.Z., 2003. Holocene yellow silt layers and the paleoclimate event of 8,200 a BP in Lop Nur, Xinjiang, NW China. Acta Geol. Sin. 77, 514–518.
Liu, M.Z., Wei, W.T., 2005. Effect of the climate change on the occurrence of dust storms in South Xinjiang since recent 60 years. Arid. Land Geogr. 28, 63–67 (in Chinese with English abstract).
Liu, J.B., Wen, Y.L., Zhao, S., Li, G.H., Jia, J., Wei, H.T., Xia, D.S., 2014. Grain-size characteristics of Kunlun Mountains loess and its environmental implication. J. Earth Environ. 5, 76–84 (in Chinese with English abstract).
Liu, S.M., 1996. A study on potential evaporation at the Tarim Basin. J. Arid Land Resour. Environ. 10, 49–55 (in Chinese with English abstract).
Liu, T., Zhang, X., Xiong, S., Qin, X., Yang, X., 2002. Glacial environments on the Tibetan Plateau and global cooling. Quat. Int. 97–98, 133–139.
Liu, Y.Z., Dong, G.R., Jin, J., Cao, Y.Q., 1994. A preliminary observation and study of dustfall in Tarim Basin. J. Desert Res. 14, 18–24 (in Chinese with English abstract).
Lu, H.Y., Guo, Z.T., 2015. Impact of climatic change and human activity on desert and sand field in northern China since the last glacial maximum. China Basic Sci 2, 3–8 (in Chinese with English abstract).
Luo, C., Peng, Z.C., Liu, W.G., Zhang, Z.F., He, J.F., Liu, G.J., Zhang, P.X., 2008. Evidence from the lacustrine sediments of lop-nur lake, northwest China for the younger Dryas event. Earth Sci. J. China Univ. Geosci. 32, 303–312 (in Chinese with English abstract).
Luo, C., Peng, Z.C., Yang, D., Liu, W.G., Zhang, Z.F., He, J.F., Chou, C.L., 2009. A lacustrine record from Lop Nur, Xinjiang, China: implications for paleoclimate change during late Pleistocene. J. Asian Earth Sci. 34, 38–45.
Lv, P., Dong, Z.B., Zhao, A.G., Zhang, K.C., 2011. Effect of shrub density on grain sizes and threshold wind velocity. J. Sediment. Res. 3, 63–66 (in Chinese with English abstract).
Ma, C.M., Wang, F.B., Cao, Q.Y., Xia, X.C., Li, S.F., Li, X.S., 2008. Climate and environment reconstruction during the medieval warm period in Lop Nur of Xinjiang, China. Chin. Sci. Bull. 53, 1942–1952.
Ma, Y., Wang, X., Huang, Z., Chen, C.Y., 2006. Change in space-time distribution of sand-dust and influence of climatic factors. Arid. Land Geogr. 29, 178–185 (in Chinese with English abstract).
Ma, Z.B., Liu, J.Q., Yuan, B.Y., Xiao, J.L., Zhang, G.P., 2004. U-series chronology of sediments associated with Late Quaternary fluctuations, Balikun Lake, northwestern China. Quat. Int. 121, 89–98.
Ma, Z.B., Cheng, H., Tan, M., Edwards, R.L., Li, H.C., You, C.F., Duan, W.H., Wang, X., Kelly, M.J., 2012. Timing and structure of the Younger Dryas event in northern China. Quat. Sci. Rev. 41, 83–93.
Maier, E., Zhang, X., Abelmann, A., Gersonde, R., Mulitza, S., Werner, M., Méheust, M., Ren, J., Chapligin, B., Meyer, H., Stein, R., Tiedemann, R., Lohmann, G., 2018. North Pacific freshwater events linked to changes in glacial ocean circulation. Nature 559, 241–258.
Martrat, B., Jimenez-Amat, P., Zahn, R., Grimalt, J.O., 2014. Similarities and dissimilarities between the last two deglaciations and interglaciations in the North Atlantic region. Quat. Sci. Rev. 99, 122–134.
McCave, I.N., Hall, I.R., Bianchi, G.G., 2006. Laser vs. settling velocity differences in silt grainsize measurements: estimation of palaeocurrent vigour. Sedimentology 53, 919–928.
Mix, A.C., Bard, E., Schneider, R., 2001. Environmental processes of the ice age: land, oceans, glaciers (EPILOG). Quat. Sci. Rev. 20, 627–657.
Nagashima, K., Tada, R., Tani, A., Sun, Y.B., Isozaki, Y., Toyoda, S., Hasegawa, H., 2011. Millennial-scale oscillations of the westerly jet path during the last glacial period. J. Asian Earth Sci. 40, 1224–1220.
North Greenland Ice-Core Project (North GRIP) Members, 2004. High resolution climate record of the northern Hemisphere reaching into the last glacial interglacial period. Nature 431, 147–151.
Oster, J.L., Ibarra, D.E., Winnick, M.J., Maher, K., 2015. Steering of westerly storms over western north America at the last glacial maximum. Nat. Geosci. 8, 201–205.
Pan, Y.B., Li, D.P., Guo, F.F., He, Z.F., Pei, J.L., Liu, J., Zhao, Y., 2008. Geomorphological features of the Keriya River valley and the early-middle Pleistocene great lake of the Tarim basin. Geol. Bull. China 27, 814–822 (in Chinese with English abstract).
Paterson, G.A., Heslop, D., 2015. New methods for unmixing sediment grain size data. Geochem. Geophys. Geosyst. 16, 4494–4506.
Peng, Y.J., Xiao, J.L., Nakamura, T., Liu, B.L., Inouchi, Y., 2005. Holocene East Asian monsoonal precipitation pattern revealed by grain-size distribution of core sediments of Daihai Lake in Inner Mongolia of north-central China. Earth Planet. Sci. Lett. 233, 467–479.
Pi, H., Sharratt, B., Lei, J.Q., 2017. Windblown sediment transport and loss in a desert–oasis ecotone in the Tarim Basin. Sci. Rep. 7, 7723. https://doi.org/10.1038/s41598-017-04971-4.
Prins, M.A., Vriend, M., Nugteren, G., Vandenberghe, J., Lu, H., Zheng, H., Weltje, G.J., 2007. Late Quaternary aeolian dust flux variability on the Chinese Loess Plateau: inferences from unmixing of loess grain-size records. Quat. Sci. Rev. 26, 230–242.
Prokopenko, A.A., Kuzmin, M.I., Williams, D.F., Gelety, V.F., Kalmychkov, G.V., Gvozdkov, A.N., Solotchin, P.A., 2005. Basin-wide sedimentation changes and deglacial lake-level rise in the Hovsgol basin, NW Mongolia. Quat. Int. 136, 59–69.
Pye, K., 1987. Aeolian Dust and Dust Deposits. Academic Press, London.
Qiang, M.R., Chen, F.H., Zhou, A.F., Xiao, S., Zhang, J.W., Jin, M., 2006. Preliminary study on dust storm events documented by grain size component of Sugan lake sediments, North Qaidam Basin. Quat. Sci. 26, 915–922 (in Chinese with English abstract).
Qiang, M., Lang, L., Wang, Z., 2010. Do fine-grained components of loess indicate westerlies: insights from observations of dust storm deposits at Lenghu (Qaidam Basin, China). J. Arid Environ. 74, 1232–1239.
Rea, D.K., Hovan, S.A., 1995. Grain size distribution and depositional processes of the mineral component of abyssal sediments: lessons from the North Pacific. Paleoceanography 10, 251–258.
Shakun, J.D., Carlson, A.E., 2009. A global perspective on Last Glacial Maximum to Holocene climate change. Quat. Sci. Rev. 29, 1801–1816.
Shi, Y., Yu, G., Liu, X., Li, B., Yao, T., 2001. Reconstruction of the 30–40 ka BP enhanced Indian monsoon climate based on geological records from the Tibetan Plateau. Palaeogeogr. Palaeoclimatol. Palaeoecol. 169, 69–83.
Stuiver, M., Reimer, P.J., Reimer, R.W., 2017. CALIB 7.0.4 [WWW program] at. http://calib.org. (Accessed 15 December 2018).
Stuut, J.B.W., Prins, M.A., Schneider, R.R., Weltje, G.J., Jansen, J.H.F., Postma, G., 2002. A 300-kyr record of aridity and wind strength in southwestern Africa: inferences from grain-size distributions of sediments on Walvis Ridge, SE Atlantic. Mar. Geol. 180, 221–233.
Sun, D., Bloemendal, J., Rea, D., An, Z., Vandenberghe, J., Lu, H., Su, R., Liu, T., 2004. Bimodal grain-size distribution of Chinese loess, and its palaeoclimatic implications. Catena 55, 325–340.
Takeuchi, N., Fujita, K., Aizen, V.B., Narama, C., Yokoyama, Y., Okamoto, S., Naoki, K., Kubota, J., 2014. The disappearance of glaciers in the tien Shan mountains in central Asia at the end of Pleistocene. Quat. Sci. Rev. 103, 26–33.
Tang, X.H., Zhong, W., Yin, H.L., 2012. Study on the characteristics of the geochemical elements and paleoclimate changes in Lake Barkol, Xinjiang since about 9.0 cal ka BP. J. South China Normal Univ. (Soc. Sci. Ed.) 44, 134–140 (in Chinese with English Abstract).
Tao, J.H., 2009. Spatial-temporal characteristics of sand-dust events and influencing factors in Northwest China. J. Desert Res. 29, 327–334 (in Chinese with English abstract).
Teng, X.H., Zhang, Z.G., Han, W.X., Fang, Y.H., Ye, C.C., 2015. Grain-size characteristics and its environmental significance of loess from southern Tarim Basin. Acta Sedimentol. Sin. 33, 941–950 (in Chinese with English abstract).
Thomas, E.R., Wolff, E., Mulvaney, R., Steffensen, J.P., Johnson, S.J., Arrowsmith, C., White, J.W.C., Vaughn, B., Popp, T., 2007. The 8.2 ka BP event from Greenland ice cores. Quat. Sci. Rev. 26, 70–81.
Vriend, M., Prins, M.A., Buylaert, J.P., Vandenberghe, J., Lu, H., 2011. Contrasting dust supply patterns across the north-western Chinese Loess Plateau during the last glacial-interglacial cycle. Quat. Int. 240, 167–180.
Wang, E.L., Liu, C.L., 2001. The Potash Resource at the Lop Nur. Geological Publishing House, Beijing, pp. 47–61 (in Chinese).
Wang, E.L., Liu, C.L., Jiao, P.C., 2006. Investigation and scientific research progress and exploitation present situation of Lop Nur salty lake potash deposits, Xinjiang, China. Geol. Rev. 52, 757–764 (in Chinese with English abstract).
Wang, M.L., Pu, Q.Y., Liu, C.L., Chen, Y., 2000. Quaternary climate and environment in the Lop Nur, Xinjiang. Acta Geol. Sin. 74, 273–278.
Wang, S.G., Wang, J.Y., Zhou, Z.J., Shang, K.Z., Yang, D.B., Zhao, Z.S., 2003. Regional characteristics of dust events in China. J. Geogr. Sci. 58, 193–200 (in Chinese with English abstract).
Wang, S.W., 2008. Glacial-interglacial cycles. Adv. Clim. Change Res. 4, 61–62 (in Chinese with English abstract).
Weltje, G.J., 1997. End-member modeling of compositional data: numerical-statistical algorithms for solving the explicit mixing problem. J. Math. Geol. 29, 503–549.
Xia, X.C., Wang, F.B., Zhao, Y.J., 2007. Lop Nur Region of China. Science Press, Beijing (in Chinese).
Xu, Z.W., Mason, J.A., Lu, H.Y., 2015. Vegetated dune morphodynamics during recent stabilization of the Mu Us dune field, north-central China. Geomorphology 228, 486–503.
Yan, S., Mu, G.J., Xu, Y.Q., 1998. Quaternary environmental evolution of the Lop Nur region, China. Acta Geograph. Sin. 332–340 (in Chinese with English abstract).
Yang, D., Luo, C., Peng, Z.C., Zhang, Z.F., Liu, W.G., Zhang, P.X., 2009. A pollen record and the paleoclimatic and environmental evolution in Lop-Nur, Xinjiang in 32.0–9.1 ka B.P. Quat. Sci. 29, 755–766 (in Chinese with English abstract).
Yang, X., Zhu, Z., Jaekel, D., Owen, L.A., Han, J., 2002. Late Quaternary palaeoenvironment change and landscape evolution along the Keriya River, Xinjiang, China: the relationship between high mountain glaciation and landscape evolution in foreland desert regions. Quat. Int. 97, 155–166.
Yang, X.P., Scuderi, L., 2010. Hydrological and climatic changes in deserts of China since the Late Pleistocene. Quat. Res. (Duluth) 73, 1–9.
Yang, X.P., Preusser, F., Radtke, U., 2006. Late Quaternary environmental changes in the Taklamakan Desert, western China, inferred from OSL-dated lacustrine and eolian deposits. Quat. Sci. Rev. 25, 923–932.
Yang, X.P., Scuderi, L., Paillou, P., Liu, Z.T., Li, H.W., Ren, X.Z., 2011. Quaternary environmental changes in the drylands of China - a critical review. Quat. Sci. Rev. 30, 3219–3233.
Yang, Y., Wang, R.J., Liu, J., Zhao, Y., Yang, Z.Y., Weng, C.Y., Wang, L., Guo, S., Zhang, T.L., 2015. Regional dust activity history during the past 45 ka reflected

by sensitive grain-size components in Lop Nur, Xinjiang. Earth Sci. Front. 22, 247–258 (in Chinese with English abstract).
Yao, T.D., Shi, Y.F., Thompson, L.G., 1992. Qilian Mountain Dunder Ice Core Records of Holocene Climate Change. Climate and Environment of Warm Period of Holocene in China. Maritime Press, Beijing, pp. 206–211 (in Chinese).
Yin, Z.Q., Qin, X.G., Wu, J.S., Ning, B., 2008. Multimodal grain-size distribution characteristics and formation mechanism of lake sediments. Quat. Sci. 28, 345–353 (in Chinese with English abstract).
Yu, G., Xue, B., Liu, J., Chen, X., 2003. LGM lake records from China and an analysis of climate dynamics using a modeling approach. Glob. Planet. Chang. 38, 223–256.
Yu, S.Y., Colman, S.M., Li, L., 2016. BEMMA: a hierarchical Bayesian end-member modeling analysis of sediment grain-size distributions. Math. Geosci. 48, 723–741.
Zhao, Y., Yu, Z.C., Liu, X.M., Zhao, C., Chen, F.H., Zhang, K., 2010. Late Holocene vegetation and climate oscillations in the Qaidam Basin of the northeastern Tibetan plateau. Quat. Res. (Duluth) 73, 59–69.
Zhao, Y.T., An, C.B., Mao, L.M., Zhao, J.J., Tang, L.Y., Zhou, A.F., Li, H., Dong, W.M., Duan, F.T., Chen, F.H., 2015. Vegetation and climate history in arid western China during MIS2: new insights from pollen and grain-size data of the Balikun Lake, eastern Tien Shan. Quat. Sci. Rev. 126, 112–125.
Zhang, G., Zhou, Y., 1992. Evaporation properties and estimates in the landlocked arid region in Xinjiang. China. Adv. Water Sci. 3, 226–232 (in Chinese with English abstract).
Zhong, W., Tuerxun, K., Shu, Q., Wang, L.G., 2005. Paleoclimatic and paleoenvironmental evolution since about 25 ka BP in the taitema lake area, south Xinjiang. Arid. Land Geogr. 28, 183–187 (in Chinese with English abstract).